Topology optimization of 2DOF piezoelectric plate energy harvester under external in-plane force

Abbas Homayouni-Amlashi, Abdenbi Mohand-Ousaid & Micky Rakotondrabe

Journal of Micro-Bio Robotics

ISSN 2194-6418

J Micro-Bio Robot
DOI 10.1007/s12213-020-00129-0

Springer

Journal of Micro-Bio Robotics
https://doi.org/10.1007/s12213-020-00129-0

RESEARCH PAPER

Topology optimization of 2DOF piezoelectric plate energy harvester under external in-plane force

Abbas Homayouni-Amlashi[1,2] · **Abdenbi Mohand-Ousaid**[2] · **Micky Rakotondrabe**[1]

Received: 8 October 2019 / Revised: 25 January 2020 / Accepted: 3 March 2020

Abstract

In this paper, the goal is to design a two degrees of freedom piezoelectric plate energy harvester which can harvest the energy from external in-plane harmonic force coming from different directions. The most challenging problem in this case is the charge cancellation due to combination of tension and compression in different parts of the plate. Therefore, topology optimization method is utilized to find the best possible layout and polarization profile of the piezoelectric plate to maximize the electrical output and to overcome the problem of charge cancellation. To do so, a detailed two dimensional finite element modelling of the piezoelectric material suitable for topology optimization is presented primarily. The topology optimization algorithm is established based on the finite element model to have minimum amount of numerical instabilities. To follow the optimized polarization profile, the electrode in top surface of the piezoelectric plate is separated to two sections that can have potentials with different sign on the same surface. Numerical simulation by COMSOL Multiphysics finite element software and experimental investigation on the fabricated designs demonstrated that the optimized design is highly superior to the classical full plate in terms of produced voltage and electrical power while having less volume of piezoelectric material.

Keywords Energy harvesting · Piezoelectric · Topology optimization

1 Introduction

In recent years, a huge part of the industrial and research budget is devoted to smart materials specially the piezoelectric materials. Thanks to their electromechanical coupling effect, they have applications in three main areas: actuation using inverse piezoelectric effect, sensing and energy harvesting using the direct piezoelectric effect. Due to their satisfying power density at small scales [14] they have applications in micro-electromechanical systems (MEMS) [15], wireless sensor networks (WSN) [33] and small scale robots [7, 26] for the purpose of sensing or energy harvesting. In the later case, although piezoelectric materials provide acceptable power densities in small scales, researchers tried to improve their performance in many ways including parametric optimization of the piezoelectric structures [21, 27], increasing the bandwidth [38], designing their structures on the basis of interval techniques [22] such that prescribed performances are robustly satisfied [13, 23], designing nonlinear and bi-stable systems [10], optimization of the electrical circuit [8], etc.

One of the recent approaches for optimization of the piezoelectric energy harvesters is using the Topology Optimization (TO) method [6]. The idea behind this method was started by integrating the Finite Element Method (FEM) to optimization methods. Later, several approach are proposed for implementation of TO algorithm. The most applicable one is the density based approach and in particular the Soild Isotropic Material with Penalization (SIMP) approach [5] which considers intermediary densities for the elements. The approach demonstrated its potential for mechanical design problems in which the goal is to minimize the structure's deformation in a predefined

✉ Abbas Homayouni-Amlashi
abbas.homayouni@femto-st.fr

Abdenbi Mohand-Ousaid
abdenbi.mohand@femto-st.fr

Micky Rakotondrabe
mrakoton@enit.fr

[1] Laboratoire Génie de Production, Nationale School of Engineering in Tarbes (ENIT), Toulouse INP, University of Toulouse, 47, Avenue d'Azereix, Tarbes, France

[2] FEMTO-ST Institute, Université Bourgogne Franche-Comté, CNRS, Besançon 25000, France

Published online: 16 March 2020

boundary and load conditions. Thereafter, several MATLAB codes are published to implement the SIMP-based TO algorithm [3, 9, 29]. For a review on published topology optimization codes, readers are referred to Ref. [37].

The idea behind the TO became interesting to optimize the piezoelectric structures. To do so, first the SIMP approach is extended for non-isotropic piezoelectric material [30]. Then, the TO methodology is employed for piezoelectric actuators and sensors [34, 35] or energy harvesters [2, 24]. For the energy harvesting applications, different cost functions and constraints are proposed to optimize the power density of the piezoelectric structure under static force [36], dynamic or harmonic force [20] and random force [18] while recent works in the field consist of coupling the electrical circuit to the optimization algorithm [25]. However, in all of the aforementioned researches, the main configuration of the piezoelectric structure is a cantilever plate in which the boundary condition is a classical clamped-free boundary condition while the applied force is a one directional bending force. This configuration is interesting for the researchers since it is easy for fabrication and experimental implementation. But it is unable to harvest the energy that comes from different directions. Most importantly, the researches devoted to integration of TO to piezoelectric energy harvesters are mostly theoretical and experimental evaluation of the TO obtained results for piezoelectric energy harvesters hardly can be found in the literature.

In this paper, the topology optimization is employed to design the layout of a piezoelectric plate that can harvest the energy from in-plane force that can comes from different directions. The volume fraction (desired optimized design volume/volume of the full piezoelectric plate) is decreased to decrease the stiffness of the piezoelectric plate against in-plane forces. In-plane forces can induce tension and compression in different parts of the piezoelectric plate which results in potential with different signs on the surface of the electrode. This phenomenon is known as charge cancellation. To remedy, the polarization direction in different parts of the plate is also optimized by the TO. The piezoelectric plate itself is a 2D structure that cannot harvest the energy from in-plane deformations due to charge cancellation. However, the proposed piezoelectric design is optimized to harvest the energy from every possible combination of deformation in X and Y direction. For this reason, the design is called a 2 Degree of Freedom (2DOF) piezoelectric energy harvester.

In terms of fabrication, having different polarization direction in a single piezoelectric plate is almost impossible. Therefore, to simulate the polarization profile obtained by TO, the surface electrode of the parts that have different polarization direction are isolated. The obtained optimized design is firstly transferred to COMSOL multi-physics software to compare the performance of the optimized design and the classical full plate design. Afterwards, the prototypes are fabricated and their performances are investigated experimentally. The results show the superiority of the optimized design over the classical full plate in terms of voltage and harvested power.

The structure of the paper is as follows: in Section 2, a detailed two dimensional finite element modelling for piezoelectric plate is presented. The FEM is presented in a way which makes it easy for implementation in TO and it reduces the numerical instability during optimization iterations. In Section 3, the implementation algorithm for piezoelectric material considering the polarization optimization is explained. Section 4 is devoted to numerical results which includes the TO results in MATLAB and simulation results by COMSOL Multiphysics software. In Section 5, the fabrication process of piezoelectric designs, the experimental setup and obtained results from experimentation are reported.

2 Modelling

2.1 2D finite element modelling of piezoelectric material

The linear coupled mechanical and electrical constitutive equation of piezoelectric materials by neglecting the thermal coupling can be written in the following compact matrix form [17]

$$\begin{aligned} \bar{T} &= c^E \bar{S} - e\bar{E} \\ \bar{D} &= e^T \bar{S} + \varepsilon^S \bar{E} \end{aligned} \tag{1}$$

In Eq. 1, $\bar{T}$ and $\bar{S}$ are the vectors of mechanical stress and strain while c^E is the mechanical stiffness tensor in constant electrical field. $\bar{D}$ and $\bar{E}$ are the vectors of electrical displacement and electrical field. e is the piezoelectric matrix while ε^S is the matrix of permittivity in constant mechanical strain and T shows the matrix transpose.

Here, the design domain is considered to be a thin piezoelectric square plate sandwiched between two electrodes. Therefore, by considering plane-stress assumption the matrices in constitutive equation (1) have this following format [12]

$$\begin{aligned} c^E &= \begin{bmatrix} c_{11}^* & c_{12}^* & 0 \\ c_{12}^* & c_{22}^* & 0 \\ 0 & 0 & c_{66}^* \end{bmatrix} \\ e^T &= \begin{bmatrix} e_{31}^* & e_{31}^* & 0 \end{bmatrix} \\ \varepsilon &= \begin{bmatrix} \varepsilon_{33}^* \end{bmatrix} \end{aligned} \tag{2}$$

where c^*_{ij}, e^*_{ij} and ε^*_{ij} are the derived elements of plane-stress form of stiffness matrix, piezoelectric coupling matrix and permittivity matrix. The derivation of the constants in matrices of Eq. 2 from full 3D matrices are explained in Appendix.

Now, to discrete the design domain and obtain the FE formulation, the four node rectangular element is employed as shown in Fig. 1. Two mechanical degrees of freedom for each node of this four nodes element is considered. To model the electrical degree of freedom it is assumed that the whole surface of the piezoelectric plate is covered by perfectly conductive electrode which brings equipotential condition. For this case, just one electrical degree of freedom is enough for each element. Therefore, the strain and electric field can be written based on the shape functions in the following form

$$\begin{aligned} \bar{S} &= B_u u \\ \bar{E} &= B_\phi \phi \end{aligned} \tag{3}$$

u and ϕ are the elemental mechanical displacement vector and electric potential value on the surface of the electrode. B_u and B_ϕ are the shape function matrices. The calculation method for mechanical strain displacement matrix (B_u) is explained in finite element method references [11]. By assuming uniform electrical field in direction of thickness aligned with the polling direction and linear variation of the potential in the thickness (h) of the piezoelectric plate [12]

$$B_\phi = 1/h \tag{4}$$

Now, by substituting equation (3) to constitutive equation (1) and utilizing the Hamilton's principle which is explained in [12, 36], after some simplification the elemental matrices are

$$\begin{aligned} k_{uu} = h\int_v B_u^T c^E B_u d\xi d\eta,\ k_{u\phi} = \int_v B_u^T e d\xi d\eta \\ k_{\phi\phi} = (\varepsilon^*_{33}A)/h,\ m = \rho h \int_v N^T N d\xi d\eta \end{aligned} \tag{5}$$

In Eq. 5, k_{uu}, $k_{u\phi}$, $k_{\phi\phi}$ and m are the elemental stiffness, piezoelectric coupling, dielectric and mass matrices respectively. A and h are the area and thickness of the elements while ρ is the density of the piezoelectric material. Now, by assembling the elemental matrices and forming the global matrices, the equation of motion can be written as.

$$\begin{bmatrix} M & 0 \\ 0 & 0 \end{bmatrix} \begin{bmatrix} \ddot{U} \\ \ddot{\Phi} \end{bmatrix} + \begin{bmatrix} K_{uu} & K_{u\phi} \\ K_{\phi u} & -K_{\phi\phi} \end{bmatrix} \begin{bmatrix} U \\ \Phi \end{bmatrix} = \begin{bmatrix} F \\ Q \end{bmatrix} \tag{6}$$

where K_{uu}, $K_{u\phi}$, $K_{\phi\phi}$ and M are the global stiffness, piezoelectric coupling, dielectric and mass matrices respectively. U and Φ are the global vectors of mechanical displacement and electrical potential. Q is the external charge and in energy harvesting applications is considered to be zero. F is the applied external harmonic force. By considering a linear electromechanical system, the input force and responses of the system can be written as

$$\begin{aligned} F &= F_0 e^{i\Omega t} \\ U = U_0 e^{i\Omega t},\ \Phi &= \Phi_0 e^{i\Omega t} \end{aligned} \tag{7}$$

in which, Ω is the excitation frequency. F_0, U_0 and Φ_0 are the amplitudes of the force, mechanical displacement and electrical potential. By substituting equation (7) to (6)

$$\begin{bmatrix} K_{uu} - M\Omega^2 & K_{u\phi} \\ K_{\phi u} & -K_{\phi\phi} \end{bmatrix} \begin{bmatrix} U \\ \Phi \end{bmatrix} = \begin{bmatrix} F \\ 0 \end{bmatrix} \tag{8}$$

Global equation of motion (8) can not be solved in this format because of the singularities in the stiffness matrices. The general approach to solve these equations

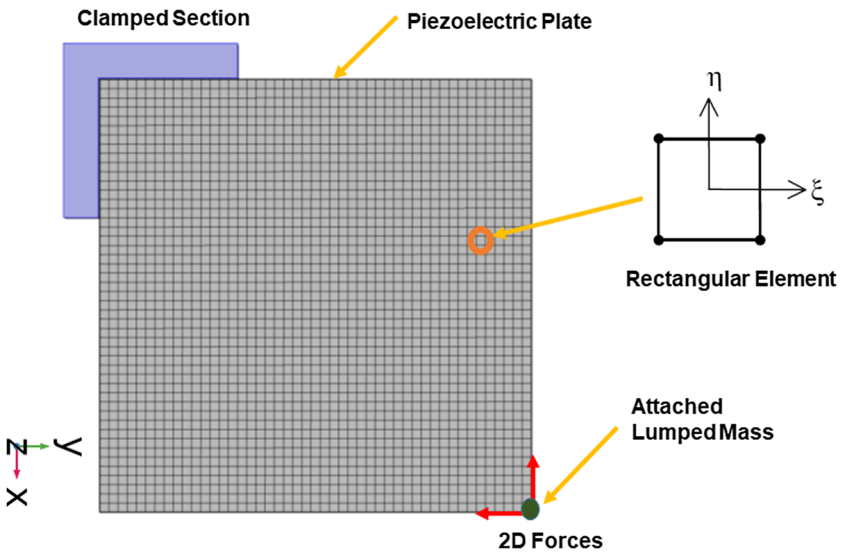

Fig. 1 Piezoelectric plate meshed with rectangular element

of motion is to apply the proper mechanical and electrical boundary conditions. In addition to singularities, there is a huge scale difference between the mechanical stiffness matrix, piezoelectric matrix and permittivity matrix which brings numerical instabilities during solving the equation and specially during the optimization. As such, before applying boundary conditions a normalization is suggested in assembling elemental matrices

$$\tilde{K}_{uu} = \frac{1}{k_0}\sum_{i=1}^{NE} k_{uu},\ \tilde{K}_{u\phi} = \frac{1}{\alpha_0}\sum_{i=1}^{NE} k_{u\phi}$$
$$\tilde{K}_{\phi\phi} = \frac{1}{\beta_0}\sum_{i=1}^{NE} k_{\phi\phi},\ \tilde{M} = \frac{1}{m_0}\sum_{i=1}^{NE} m \tag{9}$$

$(\tilde{\ })$ shows the normalization. k_0, α_0, β_0 and m_0 are the highest values of the elemental stiffness, piezoelectric coupling, dielectric and mass matrices respectively. After applying the normalization to the global matrices, the normalized global equation of motion can be written as

$$\begin{bmatrix} \tilde{K}_{uu} - \tilde{M}\tilde{\Omega}^2 & \tilde{K}_{u\phi} \\ \tilde{K}_{\phi u} & -\gamma\tilde{K}_{\phi\phi} \end{bmatrix} \begin{bmatrix} \tilde{U} \\ \tilde{\Phi} \end{bmatrix} = \begin{bmatrix} \tilde{F} \\ 0 \end{bmatrix} \tag{10}$$

where

$$\tilde{F} = F/F_0,\ \tilde{U} = U/U_0,\ ,\ \tilde{\Phi} = \Phi/\Phi_0$$
$$U_0 = F_0/k_0,\ \Phi_0 = F_0/\alpha_0$$
$$\tilde{\Omega}^2 = m_0\Omega^2/k_0,\ \gamma = k_0\beta_0/\alpha_0^2 \tag{11}$$

With applying the normalization in Eqs. 9–11 the scale difference between the matrices will be eliminated and the value γ which appears in the equation is having the scale of 10^1. This will extremely reduce the numerical instabilities when solving the equation with numerical software. Now, to solve the equation of motion in Eq. 10 boundary conditions should be applied. Application of the mechanical boundary conditions are basic FEM task [11]. For electrical boundary conditions as it is mentioned previously it is considered that electrodes on the surface of the piezoelectric plate are perfectly conductive. Hence, the equipotential condition should be applied which can be expressed in the following general form [20]

$$\tilde{\Phi} = BV_p \tag{12}$$

In general, when there are various numbers of layers for piezoelectric plates with several electrodes, B is a boolean matrix [20]. However, since here there is just one piezoelectric layer, B is a vector of ones. By applying the equipotential condition and mechanical boundary conditions the final format of the global equation of motion can be written as

$$\begin{bmatrix} \overline{K_{uu}} & \overline{K_{u\phi}} \\ \overline{K_{\phi u}} & -\overline{K_{\phi\phi}} \end{bmatrix} \begin{bmatrix} \tilde{U} \\ V_p \end{bmatrix} = \begin{bmatrix} \tilde{F} \\ 0 \end{bmatrix} \tag{13}$$

in which

$$\overline{K_{uu}} = \left[\tilde{K}_{uu} - \tilde{M}\tilde{\Omega}^2\right]_{bc}$$
$$\overline{K_{u\phi}} = \left[\tilde{K}_{u\phi}B\right]_{bc}$$
$$\overline{K_{\phi\phi}} = \gamma B^T\tilde{K}_{\phi\phi}B \tag{14}$$

where $([\ ]_{bc})$ stands for applied mechanical boundary conditions. The finite element modelling presented in Eqs. 13–14 is now ready to be used in the optimization process.

3 Topology optimization

3.1 Cost function

Generally, in the energy harvesting applications the goal is to maximize the electrical output of the system regarding the input mechanical force applied on the system. To do so, some researches defined the objective function of the optimization algorithm as the ratio of the electrical energy to the input mechanical energy (energy conversion factor) [20, 36] and other researches considered the electromechanical coupling coefficient as the objective function [1, 25]. Mathematically, these two objective functions are the same and they have the same problems. The main problem is the numerical instabilities during the optimization where to remedy, penalization of mechanical energy is suggested [25]. The other problem is the effects of penalization factors on the final topology which is discussed in [20]. For different penalization factors different layout can be obtained and in some cases the obtained layout does not have any physical meaning. Furthermore, as explained in Appendix the piezoelectric coefficients with plane-stress assumption is different to full 3d piezoelectric coefficients. Particularly, the coupling coefficient in plane-stress assumption is higher then the full piezoelectric coupling coefficient ($|e_{31}^*| > |e_{31}|$) [19]. Higher coupling coefficient brings more electromechanical coupling which is convenient for energy harvesting goal. But, it introduces numerical instabilities to the optimization and it delays the convergence of optimization algorithm. To tackle the mentioned problems, other form of cost function is defined here. To define the cost function, first the input work due to the input force can be calculated with the help of Eq. 13 as

$$W^F = \frac{1}{2}\tilde{U}^T\tilde{F} = \frac{1}{2}(\tilde{U}^T\tilde{K}_{uu}\tilde{U} + \tilde{U}^T K_{u\phi}V_p) =$$
$$\frac{1}{2}(\tilde{U}^T\tilde{K}_{uu}\tilde{U} + V_p^T\tilde{K}_{\phi\phi}V_p) \tag{15}$$

By pre-multiplying the normalized displacement vector $(\tilde{U}^T)$ to Eq. 13, it will be cleared that the input energy

to the system is converted to mechanical energy (Π^S) and electrical energy (Π^E) which are defined as

$$\Pi^S = (\frac{1}{2})\tilde{U}^T\overline{K_{uu}}\tilde{U}$$
$$\Pi^E = (\frac{1}{2})V_p^T\overline{K_{\phi\phi}}V_p \tag{16}$$

Then, the cost function can be defined in the following form,

$$J = w_j\Pi^S - (1-w_j)\Pi^E \quad 0 \le w_j \le 1 \tag{17}$$

In which the w_j is a weighting factor to determine the importance of minimizing the mechanical energy or maximizing the electrical energy. If $w_j = 1$ then the optimization problem will convert to the classical compliance problem [3, 29]. On the other hand if the w_j becomes close to zero then the final obtained topology may have no physical meaning. The cost function defined in Eq. 17, is similar to the cost function defined in [31]. Indeed, this cost function can suffer from trapping in local optima. On the other hand, it doesn't have the numerical instabilities of energy conversion factor as cost function.

The first step in gradient based optimization is to do the sensitivity analysis in which the sensitivity of cost function regarding each element should be derived. Following the same procedure presented in [36] and by considering normalized equation (13), the sensitivity of mechanical and electrical energy can be calculated as follows

$$\frac{\partial\Pi^S}{\partial x_i} = \left(\frac{1}{2}\tilde{u}_i^T + \lambda_{1,i}^T\right)\frac{\partial\left(\tilde{k}_{uu} - \tilde{m}\tilde{\Omega}^2\right)}{\partial x_i}\tilde{u}_i + \lambda_1^T\frac{\partial\tilde{k}_{u\phi}}{\partial x_i}\tilde{\phi}_i + \mu_{1,i}^T\frac{\partial\tilde{k}_{\phi u}}{\partial x_i}\tilde{u}_i - \mu_{1,i}^T\frac{\gamma\partial\tilde{k}_{\phi\phi}}{\partial x_i}\tilde{\phi}_i \tag{18}$$

$$\frac{\partial\Pi^E}{\partial x_i} = \frac{1}{2}\tilde{\phi}_i^T\frac{\partial\tilde{k}_{\phi\phi}}{\partial x_i}\tilde{\phi}_i - \mu_{2,i}^T\frac{\gamma\partial\tilde{k}_{\phi\phi}}{\partial x_i}\tilde{\phi}_i + \lambda_{2,i}^T\frac{\partial\left(\tilde{k}_{uu} - \tilde{m}\tilde{\Omega}^2\right)}{\partial x_i}u_i + \lambda_2^T\frac{\partial\tilde{k}_{u\phi}}{\partial x_i}\tilde{\phi}_i + \mu_2^T\frac{\partial\tilde{k}_{\phi u}}{\partial x_i}\tilde{u}_i \tag{19}$$

It should be noted that the sensitivity analysis is performed on the element matrices in which λ and μ are the element size adjoint vectors and $\tilde{u}_i$ and $\tilde{\phi}_i$ are the normalized elemental mechanical displacement and potential. These element size adjoint vectors can be calculated by the following global system of equation,

$$\begin{bmatrix}\overline{K_{uu}} & \overline{K_{u\phi}}\\ \overline{K_{\phi u}} & -\overline{K_{\phi\phi}}\end{bmatrix}\begin{bmatrix}\Lambda_1\\ \Upsilon_1\end{bmatrix} = \begin{bmatrix}-\overline{K_{uu}}U\\ 0\end{bmatrix}$$
$$\begin{bmatrix}\overline{K_{uu}} & \overline{K_{u\phi}}\\ \overline{K_{\phi u}} & -\overline{K_{\phi\phi}}\end{bmatrix}\begin{bmatrix}\Lambda_2\\ \Upsilon_2\end{bmatrix} = \begin{bmatrix}0\\ -\overline{K_{\phi\phi}}V_p\end{bmatrix} \tag{20}$$

In Eq. 20, Λ and Υ are the global adjoint vectors which should be resolved to give the element adjoint vectors λ and μ respectively. However, the other problem in sensitivity equations (18)–(19) is the derivative of stiffness matrices respect to element densities which leads us to the core conception of the SIMP methodology.

3.2 Solid isotropic material with penalization (SIMP)

In order to deal with the optimization problem mentioned in Eq. 17, there are several topology optimization method like binary compliance problem, Homogenization method [4] and SIMP [3, 6, 29] which is a density based approach to deal with compliance problems.

In the SIMP methodology, relative density of each element (x) can have a continuous values between 0 and 1. Therefore, in the color space of the design domain, if one considers white for the zero density and black for the density equals to one, then in the SIMP method we can have also grey elements which have densities between 0 and 1. However, the problem with grey elements is the production of the final design for the real applications. Therefore, a penalization factor is defined to push the optimized design toward the 0 and 1 structure [6]. Classical SIMP method starts by defining a relation between element density and element's young's modulus of elasticity. However, for non-isotropic piezoelectric materials the extension of this methodology can be expressed with following interpolation functions [16, 20]

$$\begin{aligned}\tilde{k}_{uu}(x,z) &= x^{p_{uu}}\tilde{k}_{uu}\\ \tilde{k}_{u\phi}(x,P) &= x^{p_{u\phi}}(2P-1)^{p_P}\tilde{k}_{u\phi}\\ \tilde{k}_{\phi\phi}(x) &= x^{p_{\phi\phi}}\tilde{k}_{\phi\phi}\\ \tilde{m}(x) &= x\tilde{m}\end{aligned} \tag{21}$$

In which, p_{uu}, $p_{u\phi}$ and $p_{\phi\phi}$ are the stiffness, coupling and permittivity penalization coefficients while (P) is the polarization. Following equations can be written for the derivatives of the stiffness matrices,

$$\begin{aligned}\frac{\partial\tilde{k}_{uu}(x)}{\partial x} &= p_{uu}x^{p_{uu}-1}\tilde{k}_{uu}\\ \frac{\partial\tilde{k}_{u\phi}(x,P)}{\partial x} &= p_{u\phi}x^{p_{u\phi}-1}(2P-1)^{p_P}\tilde{k}_{u\phi}\\ \frac{\partial\tilde{k}_{\phi\phi}(x)}{\partial x} &= p_{\phi\phi}x^{p_{\phi\phi}-1}\tilde{k}_{\phi\phi}\\ \frac{\partial\tilde{m}(x)}{\partial x} &= \tilde{m}\end{aligned} \tag{22}$$

With the help of the Eq. 22, the derivative of piezoelectric elemental matrices are calculated and can be used in the sensitivity analysis (18) and (19) . On the other hand, the piezoelectric coupling matrix ($\tilde{k}_{u\phi}$) is an interpolation function of the polarization (P) as well. This representation of piezoelectric coupling matrix comes from a methodology called "piezoelectric material with penalization and polarization" (PEMAP-P) [16] which introduces the polarization (P) as an optimization variable

that can have values between 0 and 1. In fact, this variable determines the direction of polarization. If the $(P = 1)$ then the polarization is in the positive direction of the z axis which is perpendicular to the piezoelectric plate. If $(P = 0)$ then the polarization is in the negative direction of the z axis. By introducing the polarization direction as an optimization variable then optimization algorithm finds the topology layout of the piezoelectric plate plus the polarization profile. In this case, the sensitivity of cost function respect to optimization variable (P) should also be calculated

$$\frac{\partial \Pi^S}{\partial P_i} = \lambda_1^T \frac{\partial \tilde{k}_{u\phi}}{\partial P_i}\tilde{\phi}_i + \mu_{1,i}^T \frac{\partial \tilde{k}_{\phi u}}{\partial P_i}\tilde{u}_i \tag{23}$$

$$\frac{\partial \Pi^E}{\partial P_i} = \lambda_2^T \frac{\partial \tilde{k}_{u\phi}}{\partial P_i}\tilde{\phi}_i + \mu_2^T \frac{\partial \tilde{k}_{\phi u}}{\partial P_i}\tilde{u}_i \tag{24}$$

In Eqs. 23 and 24, the adjoint vectors λ and μ come from Eq. 20. The derivative of the piezoelectric coupling matrix respect to the polarization is

$$\frac{\partial \tilde{k}_{u\phi}(x, P)}{\partial P} = 2p_P(2P-1)^{p_P-1}x^{p_{u\phi}}\tilde{k}_{u\phi} \tag{25}$$

3.3 Updating design variables

After definition of cost function and analysing the sensitivity of cost function respect to design variables, the optimization problem can be formulated as follows,

$$\begin{aligned} Minimize \quad & J = w_j \Pi^S - (1-w_j)\Pi^E \\ Subject\ to \quad & V(x) = \sum_{i=1}^{NE} x_i v_i \le V \\ & 0 < x_i \le 1 \\ & 0 \le P_i \le 1 \end{aligned} \tag{26}$$

In which, V is a volume constraint and is a fraction of the maximum possible volume. to solve the optimization problem in Eq. 26 the Method of Moving Asymptotes (MMA) [32] is utilized which can deal with multi variable and multi constraints optimization problems.

After updating the design variables in each iteration, density filter proposed in [3] is applied to avoid mesh-dependency and checkerboard patterns which are classical problems in topology optimization context.

3.4 Topology optimization algorithm

The general diagram of topology optimization method which is described above can be seen in Fig. 2. Optimization algorithm stops when there are no significant changes in design variables or energies.

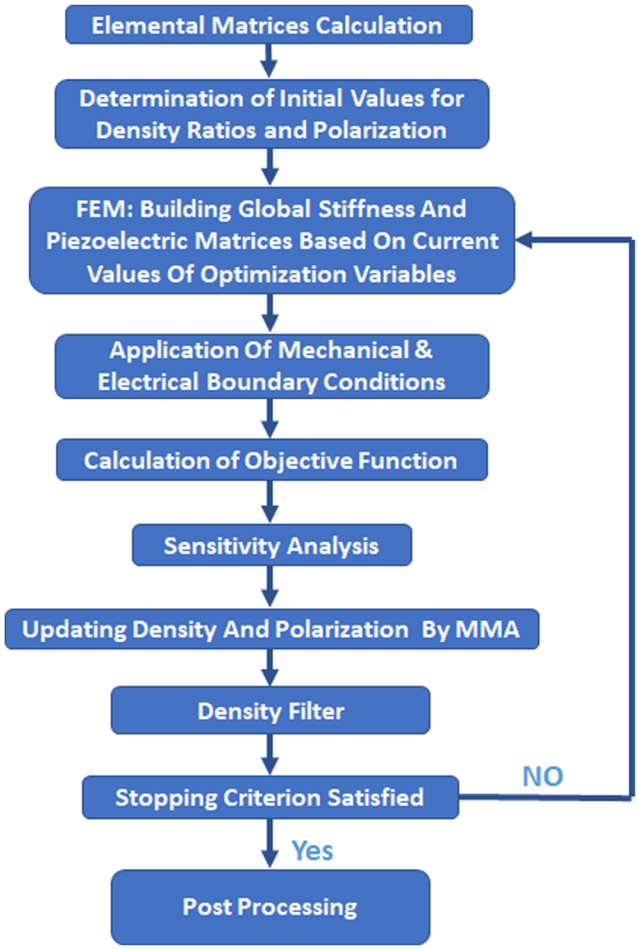

Fig. 2 Topology optimization algorithm

When the optimization stops, the next step is post processing. Actually, it is true that penalization will push the densities to zero and one. However, still in the final design, there are some grey elements. To tackle this problem, the post processing method mentioned in [28] which consist of two steps of Gaussian filter and thresholding is used here.

4 Numerical results

4.1 MATLAB FEM topology optimization

In this section, the results of TO algorithm on the design of two degrees of freedom piezoelectric plate energy harvester is presented. The specifications of the piezoelectric plate and the optimization variables are reported in Table 1.

The chosen piezoelectric material is PZT-5H which has higher coupling coefficients in comparison to other PZT material that makes it suitable for energy harvesting purposes. The ratio of thickness to length of the PZT plate

Table 1 Piezoelectric plate properties

PZT type	PZT PSI-5H4E	Volume Fraction	0.4
PZT density	7800 (kg/m^3)	Tip Magnet Weight	50 (milligram)
PZT thickness	0.254(mm)	p_{uu}	3
PZT side length	20 (mm)	$p_{u\phi}$	6
FEM number of elements	100×100	$p_{\phi\phi}$	6
Density filter radius	6	p_P	1
Clamping fraction	0.2	w_j	0.3

is 0.0127 which is well in the appropriate domain of plane-stress assumption [11]. The number of elements per length of PZT plate can be higher than chosen values. However, the chosen density filter radius can almost eliminate the mesh dependency of the final obtained layout. As such, higher number of elements will not affect the final layout. On the other hand, smaller density filter radius can lead to optimized layout with very small features which makes the fabrication procedure extremely difficult.

The clamping fraction is defined as the ratio between the length of the clamped part to the length of the square's side. This clamping fraction is chosen to be 0.2. For the same amount of applied force, by increasing the clamping fraction, the amount of electrical output energy will decrease. Although reducing the clamping fraction may seem favorable in this case, further reduction of chosen clamping part increases the stress concentration on the edge of clamping section which may lead to early fracture of the PZT plate due to applied force.

Based on the chosen volume fraction, the ratio of final optimized layout's to the full plate area is 0.4. Increasing this ratio will provide more surface of the final optimized design which increases the stiffness of the final layout against the applied force and decreases the amount of produced electrical potential. Contrarily, decreasing the volume fraction, decreases the stiffness and increases the flexibility of the optimized layout. However, The fabrication process is more complicated in this case and the design is more vulnerable against the applied force in terms of possibility of fracture.

The mass of the tip magnet is also considered as a lumped mass during FEM modelling and optimization. But the ratio of tip magnet to the PZT plate is not significant enough to affect the optimized layout within the bandwidth of the excitation frequency considered here.

Generally, the topology optimization parameters are chosen in a trial error procedure specially the penalization factors as explained by Noh et.al. [20]. But, based on the cost function defined in Eq. 26, the effects of the penalization factors on the final optimized layout are reduced. The combination of penalization factors are chosen to remove the grey elements and steer the optimized layout to black and white color space.

For choosing the weighting factor, It is obvious that the value of 0.5 gives equal weight to electrical and mechanical energies during the optimization. On the other hand, the maximum possible ratio of output electrical energy to input mechanical energy that can be found in the literature is around 0.1 [20]. So for initial guess, the weighting factor can be chosen between 0.1 and 0.5 to put more weight on increasing the output electrical energy. With performing a trial error procedure, the weighting factor of 0.3 is found. Choosing less values for weighting factor brings three main problem: 1- Mechanically unstable design due to brittleness of piezoelectric materials. 2- Obtained polarization profile will be more complicated and the fabrication process can be extremely more difficult. 3- With very low values of weighting factor, the optimization algorithm does not converge.

To start the topology optimization algorithm, the design domain, the clamped boundary condition and applied force are shown in Fig. 1. The excitation frequency is considered to be 20 Hz. Since this frequency is much smaller than the resonance frequency, considering even five times higher frequency will not affect the resulted layout. In Fig. 3, The final optimized layout and polarization profile for PZT plate under excitation of two forces in two directions can be seen. In Fig. 3b, the red color and blue color represent positive and negative polarization in z direction. The green color belongs to zero polarization which mostly belongs to areas where there is no material.

Figure 3c shows the cost function and energy ratio (electrical energy/mechanical energy) in each iteration. The final value for the energy ratio is 0.026. The biggest energy ratio reported in [20], is 0.09 for cantilever beam in bending configuration. The reason of lower energy conversion factor here is the higher stiffness of the PZT plate against in-plane forces.

As it is obvious from energy values in Fig. 3c and d, less than 100 iteration was enough to reach the convergence while optimization manually stopped at 150 iterations. The design is well converged to a black and white areas which makes the post processing step more easy to transfer the design to CAD software. The polarization profile is also clean. There are some parts which are green in the area where there are materials. In fact, these areas should be turn on to passive material based on the polarization profile. However, since these areas are not occupying a big portion of the design, they can be neglected.

After obtaining the optimized layout, the last step is devoted to post processing and transferring the obtained result to CAD and fabrication process. Therefore, the post processed and transferred design to COMSOL Multiphysics can be seen in Fig. 4. In part (b) of this figure, a separation

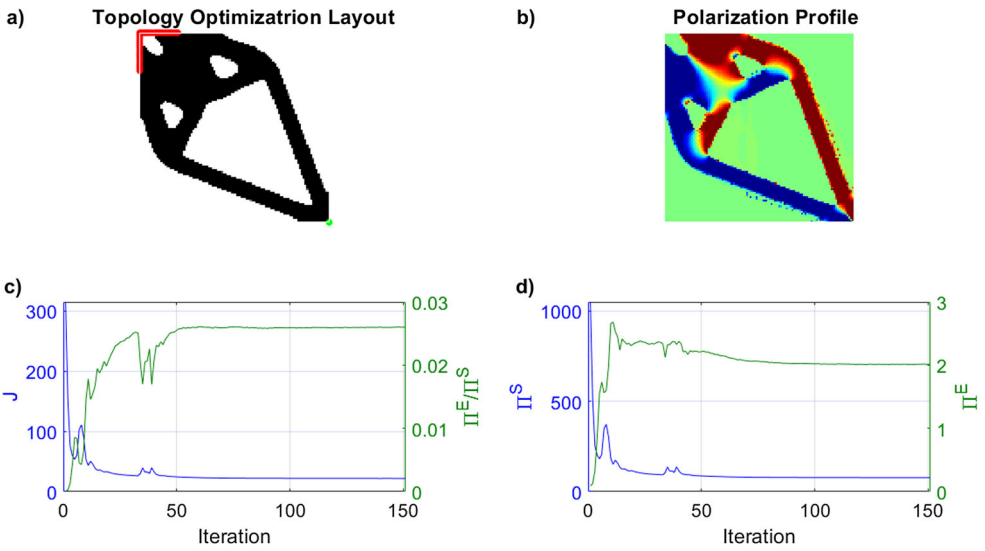

Fig. 3 Topology optimization result for 2D piezoelectric energy harvesters, **a** Density layout, **b** Optimized Polarization Profile, **c** Cost function and energy conversion factor (**d**) Mechanical and electrical energy

line can be seen that passed through the design to isolate the electrode to follow the polarization profile. In fact, this separation of electrode does not completely follow the polarization profile as it is shown in Fig. 3b. Since there is a small part on each side that the direction of polarization is the same as other part. Indeed, with the considered separation those small parts are neglected in terms of polarization. Otherwise, complete isolation of electrode based on the polarization profile makes the fabrication extremely difficult.

4.2 COMSOL multiphysics FEM simulation

To analyze the performance of the optimized design, COMSOL multiphysics is used to evaluate the voltage, electrical and mechanical energy due to applied force on the optimized design and the results are also compared with the full plate performance.

In Fig. 5, the first principal strain of the full plate and optimized design is illustrated. The important point is the better strain distribution in the optimized design in comparison to full plate. In piezoelectric material more strain is required to produce more electrical energy. Furthermore, the strain distribution in Fig. 5d, is highly similar to the obtained polarization profile in Fig. 3b. In fact, the transverse force produce compression and tension in different parts of the optimized design and the optimized polarization profile tries to avoid the charge cancellation.

In Fig. 6, the goal is to investigate the performance of the optimized design and full plate under excitation of an external force which can come from different directions. In this case, as it is obvious from Fig. 6a, the possible direction of external force is defined by angle α respect to x axis. This angle can vary from 0 to 2π and it is discretized by steps of $\pi/24$ and each point in Fig. 6d is showing these steps while the distance of the points to the center shows the amplitude of the force which is 10 (mN). The excitation frequency considered to be 20 Hz. The points in Fig. 6b, c, d and f again shows the direction of the force. However, for these parts of the figure the distance from point to the center shows the amplitude of voltage, electric power, mechanical power and power ratio respectively.

Figure 6b shows that the optimal design can have at least 3.26 times higher voltage than the full plate for the

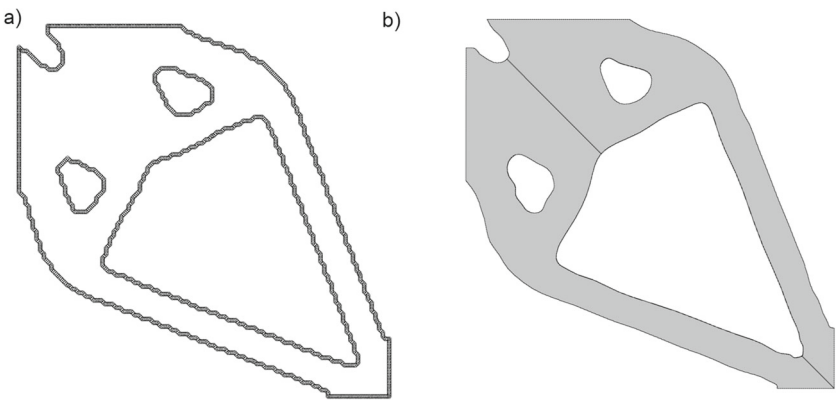

Fig. 4 Post processing of optimized design, **a** Obtained boundaries by Gaussian filter and thresholding [28], **b** Transferred design to COMSOL Multiphysics

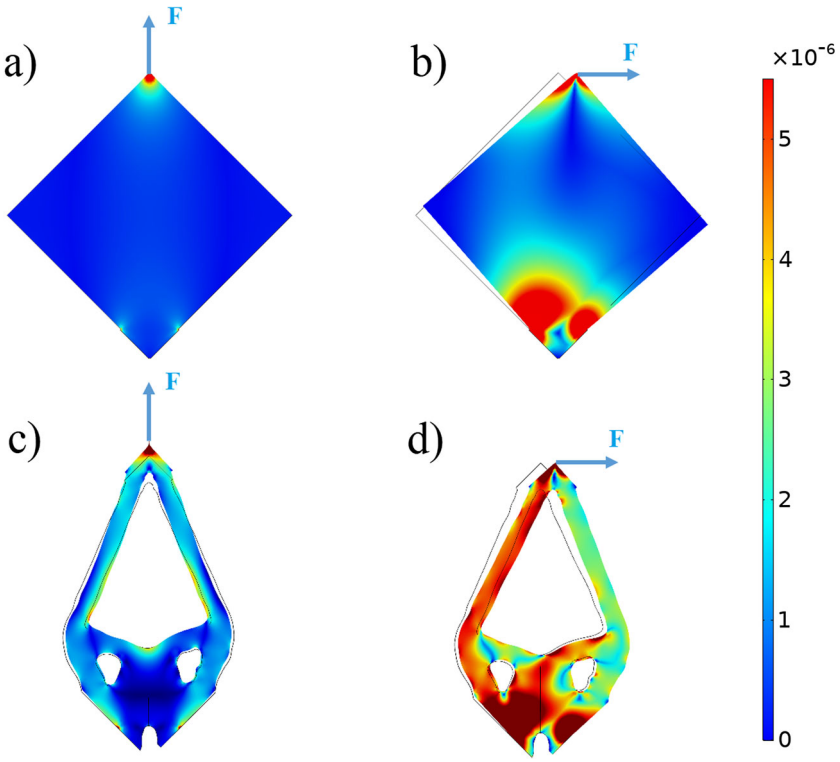

Fig. 5 Comparison of 1st principal strain in full plate and optimized design due to applied force

same amount of force and direction. The improvement of electrical power from full plate to optimal design is at least 5.2 times. While based on the part (e) of the Fig. 6 the amount of mechanical works for both of the designs are the same. As such, in terms of power ratio (electrical power/mechanical power), the optimized design is having maximum of 0.0257 energy conversion factor which is highly close to the factor obtained by topology optimization code in Fig. 3 while the maximum conversion factor for full plate is 0.0157.

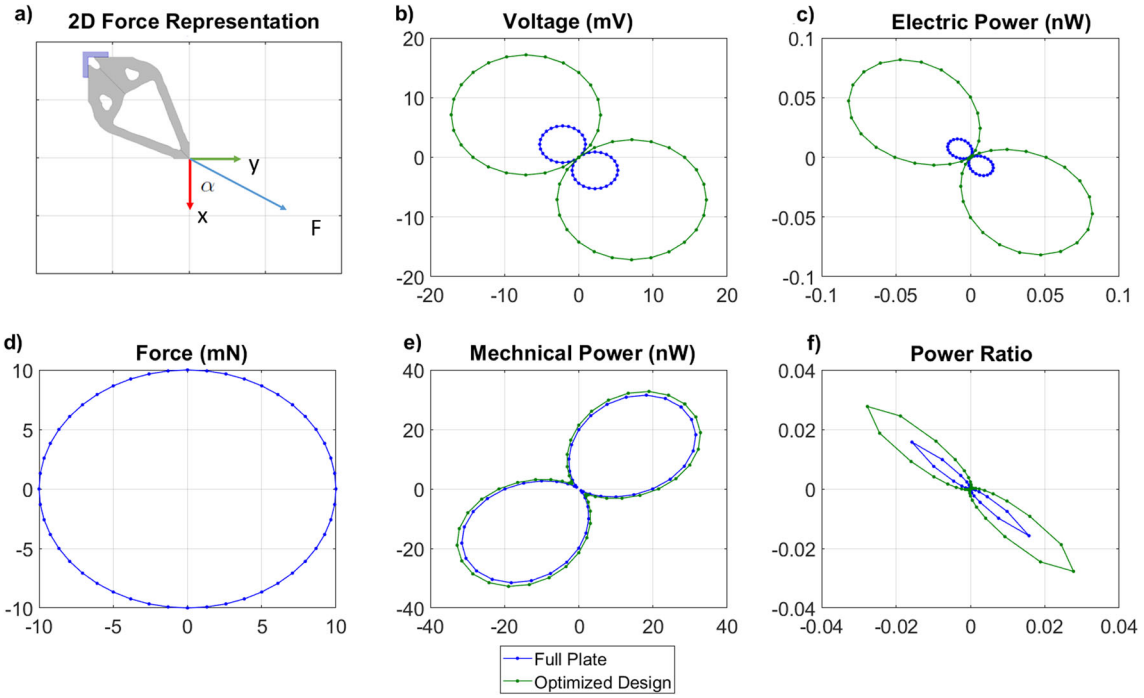

Fig. 6 COMSOL Multiphysics FEM results for piezoelectric plate under excitation by a force in different directions

Based on Fig. 6, it is obvious that the amount of produced voltage and electrical power is not the same for every direction of the force. This is due to the fact that the stiffness of the plate in different directions is not the same. As such, although the proposed optimized design is showing promising improvement in terms of electrical output in comparison to full plate, it is not harvesting the same amount of energy from every directions.

5 Experimental investigation

5.1 Fabrication

The fabrication process of designs started by cutting the designs from piezoelectric plates (commercial piezoelectric material PSI-5H4E from Piezo Systems Inc) using a laser machine (Siro Lasertec GmbH, Pforzheim, Germany). Then the wires are glued to the electrodes of the PZT plates. To do that a mixture of silver glue and epoxy is used. Then, to solidify the glue, the PZT plates with glued wires are heated inside an oven at 120 degree Celsius for two hours and then cooled down. Eventually, magnets are attached at the tip of the beam to generate vibrations force when excited by an electromagnet. As it is shown in Fig. 7b and c, the magnets are attached in two different directions so they can excite the designs in two different directions.

5.2 Experimental bench

As it is shown in Fig. 7a, the experimental setup consists of signal generator that produces sinusoidal voltage. The signal generator is connected to an electromagnet to excite the magnet attached at the tip of the designs. To clamp the designs accurately based on the defined boundary condition, 3D printed supports are utilized as it can be seen in Fig. 7b and c. The 3d supports are attached to a micropositioner which can precisely determine the distance between designs and the electromagnet. Whole setup is placed on an anti-vibration table to isolate the setup from ambient vibration. To measure the produced voltage by the design an oscilloscope (RHODE SCHWARZ, RTB 2004) with 4 input is used. To measure the current a pico ampere meter (KEYSIGHT, B2987A) is utilized.

5.3 Experimental results

In this section the goal is to measure the produced voltage and power of the optimized design and classical full plate. To guarantee the same condition during the two different

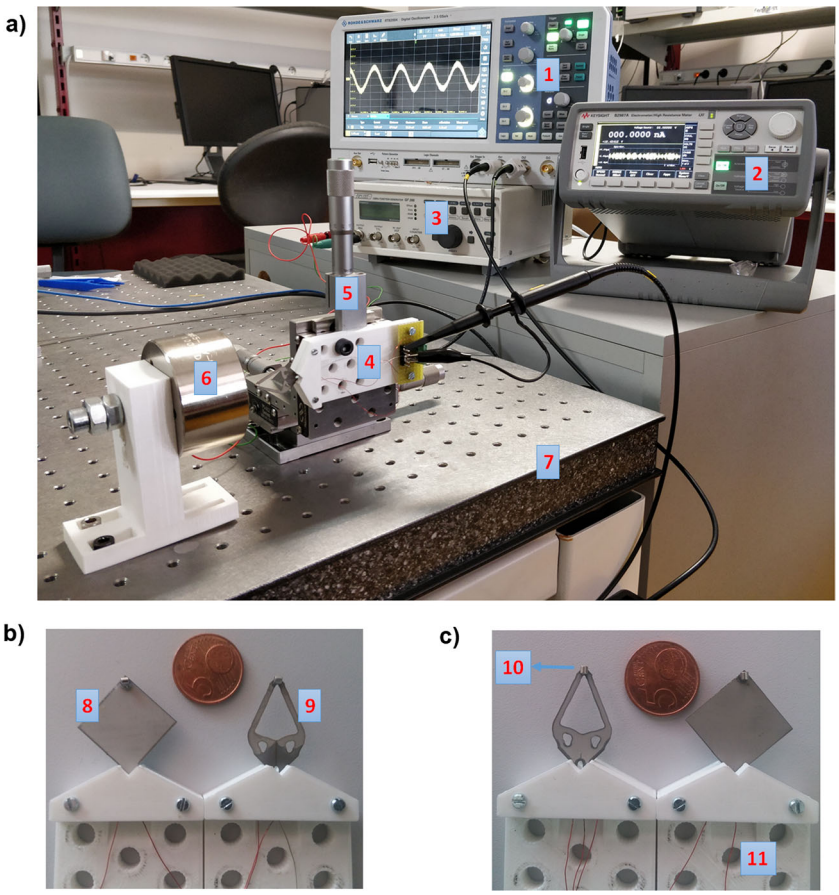

Fig. 7 **a** Experimental setup, **b** Fabricated designs, magnet direction (1), **c** Fabricated designs, magnet direction (2) . 1: Oscilloscope, 2: Pico ampere meter, 3: Signal generator, 4: Supported Design, 5: Micro positioner, 6: Electromagnet, 7: Anti-vibration table 8: Full plate design 9: Optimized design, 10: Glued magnets, 11: 3D printed supports

experiments, the micro positioner assures that the distance between the tip attached magnet and electromagnet device remains the same for optimized design and for full plate. In this case, the reported voltage and power for optimized design and full plate are for the same amount of input mechanical energy. It is worthwhile to mention that since the optimized designs have two potential electrodes, the measured voltage and power are the absolute summation of the separately measured voltage and power for each of the potential electrodes.

In the first measurements, the direction of the magnet is as shown in Fig. 7b. This direction of magnet will produce force in the direction previously shown in Fig. 5b and d. For the frequencies that varies from 20 Hz to 100 Hz the peak to peak voltage and current is measured separately. The same measurements is performed for the direction (2) of magnet which is shown in Fig. 7c. The force direction in this case is similar to the Fig. 5a and c. The measurements are shown in the Fig. 8 for optimized design and for full plate design. Based on this figure, for magnet in direction (1), the improvement from full plate to optimized design is significant. For example, for excitation frequency equal to 20 Hz, The voltage and power of optimized design are 8.75 and 7.54 times higher than the full plate. Based on the FEM simulation by COMSOL multiphysics, the expected improvements for this direction of excitation were 10 times for both power and voltage. These improvements are due to the fact that the optimized design is having better strain distribution and more importantly it has separated electrodes that avoid charge cancellation.

For direction (2) of the magnet, the voltage and power of optimized design is 3.25 and 3.82 times higher than the full plate for 20 Hz excitation frequency. Based on the FEM simulation by COMSOL multiphysics, The improvement ratios for this direction of the force in Fig. 6b and c were expected to be 3.26 and 5.2. The reduction of improvements from COMSOL Multiphysics simulation to experimental measurements can be due to fabrication process which will be discussed in next section. As it is obvious the improvement of optimized design from full plate design is more significant in the direction (1) of the magnet. In fact, for direction (2) of magnet, there is no charge cancellation in the full plate and just the optimized design is having better and higher strain distribution.

6 Discussion

Both simulation and results demonstrated promising improvement for optimized design in terms of output voltage and power. However, the gains of improvement in experimental measurements are lower than the simulation. The main reason for this reduction of improvements is the fabrication process specially, the laser cutting process. In fact, the laser beam heats up the design at the edges and the material at the vicinity of the edge can pass the curie temperature and act as passive material after. The effect of this phenomena is more extreme for the optimized design due to the fact that optimized design is having more edges in comparison to full plate. Hence, the performance of the optimized design deviates from optimum.

It is worthwhile to mention that the reported voltages and powers are not the maximum possible ones that can be obtained by the full plate and optimized design. Since, the

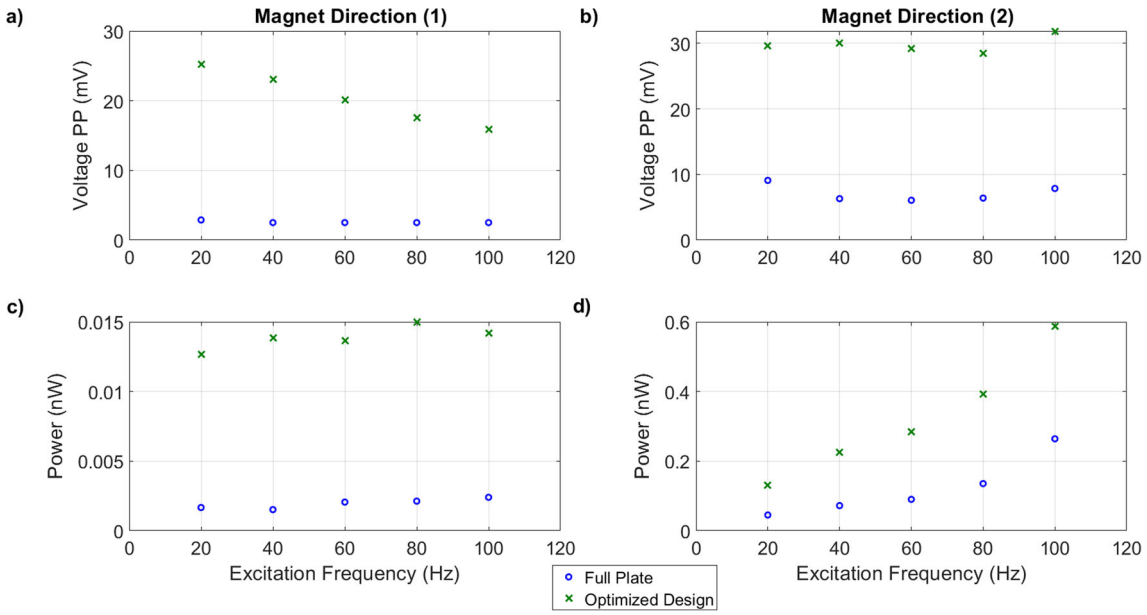

Fig. 8 Experimental Measurements for full plate design and optimized design for different excitation frequency and different magnet direction

excitation frequencies are far from resonance frequency and the applied force can be increased as well. In fact, the aim was to proof that for the same amount of mechanical input the electrical output of the optimized design is higher than the full plate. Besides, improvement in optimized design can be seen while it has less volume of material (0.4 as a volume ratio) than the full plate. As such, in terms of power density (power/volume), the gain of improvement in optimized design will be increased even more.

The placement of magnet on the piezoelectric plate can produce a negligible bending force. On the other hand, for one layer piezoelectric plate, the bending force produces no potential because of the charge cancellation that happens in the direction of the thickness [21]. But, still coming close to the bending resonance frequency which is the lowest resonance frequency may affect the in-plane excitation as well. This can be the only description for increasing the power by increasing the excitation frequency as can be seen in Fig. 8d.

Excitation at resonance frequency is not investigated in this paper. Since, the in-plane resonance frequency is extreme (more than 3200 Hz) due to high in-plane stiffness of the piezoelectric plate specially at small scale. The in-plane resonance frequency is much higher than the existence excitation frequencies in real applications.

In the literature, for the case of base excitation, usually a heavy tip attachment is considered to whether match the natural frequency to the excitation frequency or to maximize the inertia force of the attached mass. In this case, the inertia force of tip attachment can be modelled by an external tip force which is the case of the current investigation.

7 Conclusions

In this paper, a 2DOF piezoelectric plate energy harvester is designed by topology optimization method. The method of separating the electrodes is employed to follow the polarization profile and to avoid the charge cancellation. The performance of the optimized design is compared with the full plate design numerically via COMSOL Multiphysics FEM software and experimentally by fabricating the optimized design. The superiority of the optimized design in comparison to full plate design is demonstrated in harvesting energy from excitation coming from directions. The future work would consider designing 3DOF piezoelectric energy harvester that can harvest the energy coming from every possible direction in the 3D space.

Acknowledgments This work has been supported by the national CODE-TRACK project (ANR-17-CE05-0014-01, Control theory tools for optimal design of piezoelectric energy harvesters devoted to birds tracking devices). This work has also been partially supported by the Bourgogne Franche-Comté region project COMPACT.

Appendix: Plane-stress assumption for piezoelectric plate

Based on the full 3D piezoelectric constitutive equation [17] the mechanical stiffness matrix, piezoelectric matrix and permittivity matrix for a transverse isotropic material like PZT class can be written as

$$c^E = \begin{bmatrix} c_{11}^E & c_{12}^E & c_{13}^E & 0 & 0 & 0 \\ c_{12}^E & c_{11}^E & c_{13}^E & 0 & 0 & 0 \\ c_{13}^E & c_{13}^E & c_{33}^E & 0 & 0 & 0 \\ 0 & 0 & 0 & c_{44}^E & 0 & 0 \\ 0 & 0 & 0 & 0 & c_{44}^E & 0 \\ 0 & 0 & 0 & 0 & 0 & c_{66}^E \end{bmatrix}$$

$$e = \begin{bmatrix} 0 & 0 & 0 & 0 & e_{15} & 0 \\ 0 & 0 & 0 & e_{15} & 0 & 0 \\ e_{31} & e_{31} & e_{33} & 0 & 0 & 0 \end{bmatrix}$$

$$\varepsilon^S = \begin{bmatrix} \varepsilon_{11}^S & 0 & 0 \\ 0 & \varepsilon_{11}^S & 0 \\ 0 & 0 & \varepsilon_{33}^S \end{bmatrix} \tag{27}$$

Now by considering the plane-stress assumption all the nominal stresses perpendicular to the xy plane is zero [11]. Therefore, the elements of the reduced order matrices mentioned in Eq. 2 can be derived as [12]

$$c_{11}^{*E} = c_{11}^E - \frac{(c_{13}^E)^2}{c_{33}^E}, \qquad c_{12}^{E*} = c_{12}^E - \frac{(c_{13}^E)^2}{c_{33}^E}$$

$$c_{22}^{*E} = c_{22}^E - \frac{(c_{13}^E)^2}{c_{33}^E} \qquad c_{66}^{*E} = c_{66}^E$$

$$e_{31}^* = e_{31} - \frac{c_{13}^E e_{33}}{c_{33}^E}, \qquad \varepsilon_{33}^{*S} = \varepsilon_{33}^S + \frac{e_{33}^2}{c_{33}^E} \tag{28}$$

The coefficients of the PZT-5H which is fabricated for experimental investigation and the calculated plane-stress assumption is mentioned in Table 2.

Table 2 Piezoelectric coefficients

PZT PSI-5H4E		Plane-stress Assumption	
c_{11}^E	$16.9e^{10}(N/m^2)$	c_{11}^{*E}	$7.24e^{10}(N/m^2)$
c_{12}^E	$11.8e^{10}(N/m^2)$	c_{12}^{*E}	$2.14e^{10}(N/m^2)$
c_{13}^E	$10.9e^{10}(N/m^2)$	c_{22}^{*E}	$7.24e^{10}(N/m^2)$
c_{33}^E	$12.3e^{10}(N/m^2)$	-	-
c_{66}^E	$2.5e^{10}(N/m^2)$	c_{66}^{*E}	$2.5e^{10}(N/m^2)$
e_{31}	$-12(C/m^2)$	e_{31}^*	$-28.12(C/m^2)$
e_{33}	$18.2(C/m^2)$	-	-
ε_{33}^S	$1390 \times \varepsilon_0$	ε_{33}^{*S}	$1694 \times \varepsilon_0$

References

1. de Almeida BV, Cunha DC, Pavanello R (2019) Topology optimization of bimorph piezoelectric energy harvesters considering variable electrode location. Smart Materials and Structures
2. Amlashi AH, Mohand-Ousaid A, Rakotondrabe M (2019) Topology optimization of piezoelectric plate energy harvester under external in-plan force considering different boundary conditions. In: 2019 International conference on manipulation, automation and robotics at small scales (MARSS). IEEE, pp 1–6
3. Andreassen E, Clausen A, Schevenels M, Lazarov BS, Sigmund O (2011) Efficient topology optimization in matlab using 88 lines of code. Struct Multidiscip Optim 43(1):1–16
4. Bendsøe MP, Kikuchi N (1988) Generating optimal topologies in structural design using a homogenization method. Comput Methods Appl Mech Eng 71(2):197–224
5. Bendsøe MP, Sigmund O (1999) Material interpolation schemes in topology optimization. Arch Appl Mech 69(9-10):635–654
6. Bendsoe MP, Sigmund O (2013) Topology optimization theory, methods and applications. Springer Science & Business Media
7. Cha Y, Hong S (2016) Energy harvesting from walking motion of a humanoid robot using a piezoelectric composite. Smart Mater Struct 25(10):10LT01
8. Chamanian S, Ulusan H, Koyuncuoglu A, Muhtaroglu A, Kulah H (2018) An adaptable interface circuit with multi-stage energy extraction for low power piezoelectric energy harvesting mems. IEEE Transactions on Power Electronics
9. Chen Q, Zhang X, Zhu B (2019) A 213-line topology optimization code for geometrically nonlinear structures. Struct Multidiscip Optim 59(5):1863–1879
10. Harne R, Wang K (2013) A review of the recent research on vibration energy harvesting via bistable systems. Smart Mater Struct 22(2):023001
11. Hutton DV, Wu J (2004) Fundamentals of finite element analysis, vol 1. McGraw-hill, New York
12. Junior CDM, Erturk A, Inman DJ (2009) An electromechanical finite element model for piezoelectric energy harvester plates. J Sound Vib 327(1–2):9–25
13. Khadraoui S, Rakotondrabe M, Lutz P (2014) Optimal design of piezoelectric cantilevered actuators with guaranteed performances by using interval techniques. Trans Mechatron 19(5):1660–1668
14. Kim HS, Kim J, Kim J (2011) A review of piezoelectric energy harvesting based on vibration. Int J Precis Eng Manuf 12(6):1129–1141
15. Kim SG, Priya S, Kanno I (2012) Piezoelectric mems for energy harvesting. MRS Bull 37(11):1039–1050
16. Kögl M, Silva EC (2005) Topology optimization of smart structures: design of piezoelectric plate and shell actuators. Smart Mater Struct 14(2):387
17. Lerch R (1990) Simulation of piezoelectric devices by two- and three-dimensional finite elements. IEEE Trans Ultrason Ferroelectr Frequency Control 37(3):233–247
18. Lin ZQ, Gea HC, Liu ST (2011) Design of piezoelectric energy harvesting devices subjected to broadband random vibrations by applying topology optimization. Acta Mech Sinica 27(5):730
19. Muralt P (1997) Piezoelectric thin films for mems. Integr Ferroelectr 17(1-4):297–307
20. Noh JY, Yoon GH (2012) Topology optimization of piezoelectric energy harvesting devices considering static and harmonic dynamic loads. Adv Eng Softw 53:45–60
21. Rabenorosoa K, Rakotondrabe M (2015) Performances analysis of piezoelectric cantilever based energy harvester devoted to mesoscale intra-body robot. In: Next-generation robotics II; and machine intelligence and bio-inspired computation: theory and applications IX, vol 9494. International Society for Optics and Photonics, p 94940E
22. Rakotondrabe M (2011) Performances inclusion for stable interval systems, pp 4367–4372
23. Rakotondrabe M (2013) Design of piezoelectric actuators with guaranteed performances using the performances inclusion theorem and interval tools, a Chapter in 'Smart materials-based actuators at the micro/nano-scale: characterization, control and applications'. Springer
24. Rupp CJ, Evgrafov A, Maute K, Dunn ML (2009) Design of piezoelectric energy harvesting systems: a topology optimization approach based on multilayer plates and shells. J Intell Mater Syst Struct 20(16):1923–1939
25. Salas R, Ramírez F, Montealegre-Rubio W, Silva E, Reddy J (2018) A topology optimization formulation for transient design of multi-entry laminated piezocomposite energy harvesting devices coupled with electrical circuit. Int J Numer Methods Eng 113(8):1370–1410
26. Salazar R, Taylor G, Khalid M, Abdelkefi A (2018) Optimal design and energy harvesting performance of carangiform fish-like robotic system. Smart Mater Struct 27(7):075045
27. Schlinquer T, Mohand-Ousaid A, Rakotondrabe M (2017) Optimal design of a unimorph piezoelectric cantilever devoted to energy harvesting to supply animal tracking devices. IFAC-PapersOnLine 50(1):14600–14605
28. Schlinquer T, Mohand-Ousaid A, Rakotondrabe M (2018) Displacement amplifier mechanism for piezoelectric actuators design using simp topology optimization approach. In: IEEE int conference on robotics and automation. IEEE, pp 1–7
29. Sigmund O (2001) A 99 line topology optimization code written in matlab. Struct Multidiscip Optim 21(2):120–127
30. Silva EN, Fonseca JO, Kikuchi N (1997) Optimal design of piezoelectric microstructures. Comput Mech 19(5):397–410
31. Silva EN, Nishiwaki S, Kikuchi N (2000) Topology optimization design of flextensional actuators. IEEE Trans Ultrasonics Ferroelectr Frequency Control 47(3):657–671
32. Svanberg K (1987) The method of moving asymptotes—a new method for structural optimization. Int J Numer Methods Eng 24(2):359–373
33. Toprak A, Tigli O (2014) Piezoelectric energy harvesting: state-of-the-art and challenges. Appl Phys Rev, 1(3)
34. Zhang X, Kang Z (2014) Dynamic topology optimization of piezoelectric structures with active control for reducing transient response. Comput Methods Appl Mech Eng 281:200–219
35. Zhang X, Kang Z (2014) Topology optimization of piezoelectric layers in plates with active vibration control. J Intell Mater Syst Struct 25(6):697–712
36. Zheng B, Chang CJ, Gea HC (2009) Topology optimization of energy harvesting devices using piezoelectric materials. Struct Multidiscip Optim 38(1):17–23
37. Zhu B, Zhang X, Zhang H, Liang J, Zang H, Li H, Wang R (2020) Design of compliant mechanisms using continuum topology optimization: a review. Mech Mach Theory 143:103622
38. Zhu D, Tudor MJ, Beeby SP (2009) Strategies for increasing the operating frequency range of vibration energy harvesters: a review. Measur Sci Technol 21(2):022001